The Astrophysical Journal, 891:76 (7pp), 2020 March 1 https://doi.org/10.3847/1538-4357/ab7228
© 2020. The American Astronomical Society. All rights reserved.

# Black Hole Mass Function and Its Evolution—The First Prediction for the Einstein Telescope

Xuheng Ding[1,2], Kai Liao[3], Marek Biesiada[4,5], and Zong-Hong Zhu[1,4]
[1] School of Physics and Technology, Wuhan University, Wuhan 430072, People's Republic of China; zhuzh@whu.edu.cn
[2] Department of Physics and Astronomy, University of California, Los Angeles, CA 90095-1547, USA
[3] School of Science, Wuhan University of Technology, Wuhan 430070, People's Republic of China
[4] Department of Astronomy, Beijing Normal University, Beijing 100875, People's Republic of China
[5] National Centre for Nuclear Research, Pasteura 7, 02-093 Warsaw, Poland
*Received 2019 September 2; revised 2020 January 17; accepted 2020 January 30; published 2020 March 5*

## Abstract

Knowledge of the black hole mass function (BHMF) and its evolution would help us understand the origin of BHs and how BH binaries formed at different stages in the history of the universe. We demonstrate the ability of a future third-generation gravitational-wave (GW) detector—the Einstein Telescope (ET)—to infer the slope of the BHMF and its evolution with redshift. We perform a Monte Carlo simulation of the measurements of chirp signals from binary BH systems (BBH) that could be detected by ET, including the BH masses and their luminosity distances ($d_L$). We use the mass of a primary black hole in each binary system to infer the BHMF as a power-law function with slope parameter $\alpha$. Taking into account the bias that could be introduced by the uncertainty of measurements and by the selection effect, we carried out the numerical tests and found that only 1000 GW events registered by ET ($\sim$1% of its yearly detection rate) could accurately infer the $\alpha$ with a precision of $\alpha \sim 0.1$. Furthermore, we investigate the validity of our method to recover a scenario where $\alpha$ evolves with redshift as $\alpha(z) = \alpha_0 + \alpha_1 \frac{z}{1+z}$. Taking a thousand GW events and using $d_L$ as the redshift estimator, our tests show that one could infer the value of evolving parameter $\alpha_1$ accurately at the uncertainty level of $\sim$0.5. Our numerical tests verify the reliability of our method. The uncertainty levels of the inferred parameters can be trusted directly for several sets of the parameters we assumed, yet they should not be treated as general.

*Unified Astronomy Thesaurus concepts:* Gravitational waves (678); Black holes (162)

## 1. Introduction

The masses of astrophysical black holes (BHs) are known to cover a wide range, from stellar to supermassive ($\sim 10^{10} M_\odot$). The discovery of coalescing binary black holes (BBHs) in the LIGO gravitational-wave (GW) detectors provided substantial evidence of stellar-mass BHs (The LIGO Scientific Collaboration & The Virgo Collaboration 2016a), while supermassive BHs are supposed to exist in the centers of almost all galaxies (Lynden-Bell 1969; Kormendy & Richstone 1995). GWs provide a direct way to study inspiralling BBH systems, enabling derivation of their basic parameters including mass, spin, and luminosity distances (The LIGO Scientific Collaboration & The Virgo Collaboration 2017, 2019a). This creates the opportunity to not only measure the properties of BHs (The LIGO Scientific Collaboration & The Virgo Collaboration 2019b), but also answer some fundamental questions concerning cosmography (Cai & Yang 2017; Liao et al. 2017; Ding et al. 2019), GW speed (Collett & Bacon 2017; Fan et al. 2017), or strong lensing of GWs (Piórkowska et al. 2013; Biesiada et al. 2014; Ding et al. 2015).

Nevertheless, it is still unclear how BHs formed (Fryer 1999; Fryer & Kalogera 2001; Mirabel 2017). In particular, the number and mass distribution of stellar-mass BHs in the universe still need to be clarified. The recent detections of GW events have launched a new era of gravitational-wave astronomy (e.g., The LIGO Scientific Collaboration & The Virgo Collaboration 2016a, 2016b, 2019a) and provided new opportunities to study BBH system formation channels. At present, however, observations cannot firmly select basic formation scenarios like the evolution of isolated pairs of stars (Bethe & Brown 1998; Portegies Zwart & Yungelson 1998), chemically homogeneous evolution (de Mink & Mandel 2016; Marchant et al. 2016), dynamic binary formation in dense clusters (Kulkarni et al. 1993; Portegies Zwart & McMillan 2000), and other channels introduced in The LIGO Scientific Collaboration & The Virgo Collaboration (2019b). Inferring distributions of BH mass could be the key to distinguishing these scenarios and learning more about the physical process and evolutionary environment of binary BH formation.

The current GWTC-1 catalog of binary coalescences detected by LIGO/Virgo GW interferometers includes 10 BH–BH binaries and 1 neutron star binary (NS–NS; GW170817) binary (The LIGO Scientific Collaboration & The Virgo Collaboration 2019a). Assuming the BH mass function (BHMF) is parameterized as a two-sided truncated power law, Kovetz et al. (2017) estimated that further LIGO measurements would provide thousands of BBHs and constrain the BHMF slope parameter $\alpha$ at 10% precision. More recently, the LIGO collaboration has used 10 BBH merger events and constrained the BHMF power-law index to $\alpha = 1.6^{+1.5}_{-1.7}$ (90% credibility; The LIGO Scientific Collaboration & The Virgo Collaboration 2019b). In the next decade, the number of detected coalescences of BBH systems is expected to be increase rapidly with improvements of the detector sensitivities. Particularly, the third-generation gravitational-wave detector Einstein Telescope (ET) is capable of detecting $10^4$–$10^8$ coalescing BBHs per year (Abernathy et al. 2011). Moreover, since this instrument could detect GW events from the distant universe up to $z \sim 17$ (Abernathy et al. 2011), the wide redshift range of the BBH inspiral events enables us to study $\alpha$ as a function of redshift. In this study, we use the Monte Carlo (MC) approach to simulate GW events from BBH

mergers that could be measured by the ET. We construct a mock BBH merger catalog to examine their ability to constrain the BHMFs, taking into account the data noise level and selection bias realistically.

This paper is organized as follows. In Section 2 we describe the simulation of the BBH inspiral events detectable by ET using the MC approach. In this section, we assume the initial assumptions for the BH mass function used further as true values to be recovered from the data. In Section 3, we introduce the theoretical framework to reconstruct the BHMFs, considering the noise realization and the selection effects. Furthermore, we take a further step by considering the power-law index $\alpha$ as a function of redshift and explore how to use luminosity distance as a redshift estimator and detect such evolution. We present our results in Section 4. The discussion and conclusions are given in Section 5. Throughout this paper, we assume a standard concordance cosmology with $H_0 = 70\ \mathrm{km\ s^{-1}\ Mpc^{-1}}$, $\Omega_m = 0.30$, and $\Omega_\Lambda = 0.70$.

## 2. Data Simulation

In this section we describe the simulation of a realistic mock catalog of GW signals from BBHs detectable by the future ET interferometric detector. Numerical predictions of BBH inspirals detectable by ET have been discussed in many works, and it has been forecasted that the yearly detection rate of BBHs would be of order $\sim 10^{4-8}$ (Abernathy et al. 2011) or at least $\sim 10^5$ according to less optimistic yet realistic scenarios (Piórkowska et al. 2013; Biesiada et al. 2014). More recently, Yang et al. (2019) developed the approach of a MC simulation to predict the detection rate by explicitly considering each BBH inspiral event sampled from the outcome of the population synthesis model, which provides a way to mimic a realistic BBH GW catalog. The backbone of this approach is to use random seeds to build up a mock universe that includes a sufficient volume of BBH inspiral events with essential parameters that are related to this study. For further details, see Yang et al. (2019, Section 2, therein); we provide a brief summary of the key points below.

### 2.1. Detection Criteria

For a specific BBH inspiral event at redshift $z_s$, the ET's corresponding signal-to-noise ratio $\rho$ is defined as (Abernathy et al. 2011)

$$\rho = 8\Theta \frac{r_0}{d_L(z_s)} \left( \frac{(1+z)\mathcal{M}_0}{1.2 M_\odot} \right)^{5/6} \sqrt{\zeta(f_{\max})}, \quad (1)$$

where $r_0$ is the detector's characteristic distance parameter and $\zeta(f_{\max})$ is the dimensionless function reflecting the overlap between the GW signal and the ET's effective bandwidth. For simplicity, we followed Taylor & Gair (2012) and approximated $\zeta(f_{\max})$ as unity. $\mathcal{M}_0$ is the intrinsic chirp mass defined as $\mathcal{M}_0 = \frac{(m_1 m_2)^{3/5}}{(m_1+m_2)^{1/5}}$, where $m_1$ and $m_2$ are the respective masses of the BBH components. $\Theta$ is the orientation factor determined by four angles as (Finn & Chernoff 1993)

$$\Theta = 2[F_+^2(1+\cos^2\iota)^2 + 4F_\times^2 \cos^2\iota]^{1/2}, \quad (2)$$

where: $F_+ = \frac{1}{2}(1+\cos^2\theta)\cos 2\phi \cos 2\psi - \cos\theta \sin 2\phi \sin 2\psi$, and $F_\times = \frac{1}{2}(1+\cos^2\theta)\sin 2\phi \cos 2\psi + \cos\theta \sin 2\phi \cos 2\psi$ are so-called antenna patterns. The four angles $(\theta, \phi, \psi, \iota)$ respectively describe the direction to the BBH system relative to the detector and the binary orientation relative to the line of sight between it and the detector. They are independent and one can assume that they are $(\cos\theta, \phi/\pi, \psi/\pi, \cos\iota)$ distributed uniformly over the range $[-1, 1]$. The GW signal is considered detectable if its $\rho$ is over the detecting threshold, i.e., $\rho > \rho_0 = 8$.

### 2.2. MC Approach

We aim to build up a sufficient volume of BBH systems in the mock universe by randomly generating the key parameters for each BBH system as specified below. The first key parameter is the redshift $z_s$. We sample the merging BBH systems according to the yearly merger rate in a redshift interval $[z_s, z_s + dz_s]$:

$$d\dot{N}(z_s) = 4\pi \left( \frac{c}{H_0} \right)^3 \frac{\dot{n}_0(z_s)}{1+z_s} \frac{\tilde{r}^2(z_s)}{E(z_s)} dz_s. \quad (3)$$

where the intrinsic BBH merger rate $\dot{n}_0(z_s)$ is the one predicted by the population synthesis model (using `StarTrack` code[6]) in Dominik et al. (2013), $\tilde{r}(z_s)$ is the dimensionless comoving distance to the source, and $E(z_s)$ is the dimensionless expansion rate of the universe at redshift $z_s$. Other key parameters include the four angles $(\theta, \phi, \psi, \iota)$ in the Equation (2) and the masses of each BH in the binary system (i.e., $m_1$ and $m_2$). For the purpose of randomly generating the BH masses, we follow the previous works (Kovetz et al. 2017; Fishbach et al. 2018; The LIGO Scientific Collaboration & The Virgo Collaboration 2019b) and assume that $m_1$ follows a power-law distribution with a hard cut at both maximum and minimum mass:

$$P(m_1|\alpha, M_{\max}, M_{\min}) = m_1^\alpha \mathcal{H}(m_1 - M_{\min}) \mathcal{H}(M_{\max} - m_1), \quad (4)$$

where $\mathcal{H}$ is the Heaviside step function. Then, the secondary mass, $m_2$, is sampled from a uniform distribution between $[M_{\min}, m_1]$. Let us note that we only take $m_1$ to reconstruct the BHMF, thus the assumption of the distribution for $m_2$ actually does not affect the inference for the shape of BHMF. For the purpose of the simulation, however, all these parameters are necessary to determine the value of $\Theta$ and $\mathcal{M}_0$ in Equation (1). We combine them with their redshift $z_s$ to generate the $\rho$ of each BBH inspiraling system. We only collect events that have $\rho > \rho_0 = 8$, meaning that events with $\rho < 8$ are too faint to detect.

Concerning the BHMF we consider two scenarios. In the first scenario, the exponent $\alpha$ is constant, hence the shape of the BHMF is fixed throughout the redshift range probed by the ET. In the second scenario, we consider that $\alpha$ varies as a function of redshift according to

$$\alpha(z) = \alpha_0 + \alpha_1 \frac{z}{1+z}, \quad (5)$$

such that the $\alpha(z)$ would transform gradually from $\alpha_0$ to $\alpha_0 + \alpha_1$ through low $z$ to high $z$. We do not have any clear physical precedent for how could $\alpha$ evolve with redshift, particularly which analytical expression would describe it

[6] The data are taken from http://www.syntheticuniverse.org.

reliably. Therefore, the above ansatz is actually a suitable form of the first-order Taylor expansion of $\alpha$ as a function of the scale factor $a$ (around the present value $a(t_0) = 1$, where $a(t) = \frac{1}{1+z}$).

### 2.3. Estimation of Parameter Error

We aim to produce the mock data set of the future GW events representative of the ET measurements. In order to consider the measurement uncertainties in a realistic way, we distribute random statistical uncertainties into the simulated data as described below.

The quantities measurable from the BBH inspiral waveform are comprised of $d_L$, redshifted chirp mass $(1+z)\mathcal{M}_0$ and $\rho$. Individual masses $m_1$ and $m_2$ are derived from the combination of the chirp mass and the total mass $m_1+m_2$, which can also be extracted from the chirp waveform. Let us note that physical quantities inferred from the LIGO detections had asymmetric upper and lower uncertainty limits, hence they followed the *skewed* distributions. Therefore, instead of the symmetric Gaussian distribution, we assume that the simulated mock measurements follow the log-normal distribution with a standard deviation of $\mathcal{M}_0$, $d_L$, and $m_1$ equal to 0.17, 0.35, and 0.2, respectively. For instance, if $m_{1,\mathrm{fid}}$ is the true value for $m_1$, the probability density used to simulate the measured value is

$$P(m_1) = \frac{1}{m_1\sigma_{m_1}\sqrt{2\pi}}\exp\left[-\frac{\log(m_1) - \log(m_{1,\mathrm{fid}})}{2\sigma_{m_1}}\right]. \quad (6)$$

We set up the uncertainties for $\mathcal{M}_0$, $d_L$, and $m_1$ by taking the results of Ghosh et al. (2016) as a reference, who explored the expected statistical uncertainties with which the parameters of BH binaries can be measured from GW observations by next-generation ground-based GW observatories. Note that the assumed uncertainty level of these quantities only affects the uncertainty of the inferred parameters (i.e., the precision) and would not affect the validity test of our method (i.e., the accuracy).

Having clarified the MC approach and defined the data's uncertainty level, we are capable of producing the mock GW data set. For the purposes of demonstration, we list an example of 1000 BBH inspiral events as simulated in one realization of the MCMC seeding process.

## 3. Theoretical Framework

In this section, we describe the fitting procedure for the parameterized BHMFs. In principle, the modeling for a data set that follows a power-law distribution like that Equation (4) is very straightforward. To derive the posterior of the parameters, one only needs to combine all the measured median values together in a joint likelihood:

$$P(\alpha, M_{\max}, M_{\min}|m_1) \propto \prod_{i=1}^{\mathrm{total}} P(m_{1,i}|\alpha, M_{\max}, M_{\min}) \quad (7)$$

where $m_{1,i}$ is the primary mass inferred from the $i$th GW event. However, the median values of simulated $m_1$, as shown in Table 1, actually deviate from the initial power-law distribution. This deviation stems from several real effects. In Sections 3.1 and 3.2, we introduce them and explore how to account for them.

**Table 1**
Illustration of the Mock GW Catalog

| Object ID | $m_1$ ($M_\odot$) | Luminosity Distance (Mpc) | Chirp Mass ($M_\odot$) | SNR ($\rho$) |
|---|---|---|---|---|
| (1) | (2) | (3) | (4) | (5) |
| ID1 | $8.14^{+1.80}_{-1.48}$ | $25356.8^{+5614.1}_{-4596.4}$ | $9.91^{+2.19}_{-1.80}$ | 18.512 |
| ID2 | $43.93^{+9.73}_{-7.96}$ | $12956.9^{+2868.7}_{-2348.7}$ | $28.64^{+6.34}_{-5.19}$ | 46.953 |
| ID3 | $5.05^{+1.12}_{-0.92}$ | $8617.6^{+1908.0}_{-1562.1}$ | $3.60^{+0.80}_{-0.65}$ | 9.836 |
| ID4 | $13.93^{+3.08}_{-2.53}$ | $47473.1^{+10510.7}_{-8605.4}$ | $10.97^{+2.43}_{-1.99}$ | 17.563 |
| ID5 | $11.37^{+2.52}_{-2.06}$ | $21485.0^{+4756.8}_{-3894.6}$ | $10.68^{+2.36}_{-1.94}$ | 31.107 |
| ID6 | $21.67^{+4.80}_{-3.93}$ | $9446.1^{+2091.4}_{-1712.3}$ | $7.64^{+1.69}_{-1.39}$ | 31.624 |
| ID7 | $32.20^{+7.13}_{-5.84}$ | $69317.4^{+15347.1}_{-12565.1}$ | $19.35^{+4.28}_{-3.51}$ | 13.496 |
| ID8 | $7.73^{+1.71}_{-1.40}$ | $25104.5^{+5558.2}_{-4550.7}$ | $6.68^{+1.48}_{-1.21}$ | 9.612 |
| ID9 | $35.63^{+7.89}_{-6.46}$ | $16321.8^{+3613.7}_{-2958.6}$ | $10.96^{+2.43}_{-1.99}$ | 16.202 |
| ID10 | $18.78^{+4.16}_{-3.40}$ | $54375.1^{+12038.8}_{-9856.5}$ | $15.16^{+3.36}_{-2.75}$ | 29.232 |
| ... | ... | ... | ... | ... |
| ID991 | $29.40^{+6.51}_{-5.33}$ | $40765.1^{+9025.5}_{-7389.5}$ | $29.79^{+6.59}_{-5.40}$ | 28.134 |
| ID992 | $6.41^{+1.42}_{-1.16}$ | $16026.7^{+3548.4}_{-2905.2}$ | $4.54^{+1.01}_{-0.82}$ | 17.550 |
| ID993 | $10.27^{+2.27}_{-1.86}$ | $33207.9^{+7352.3}_{-6019.6}$ | $8.57^{+1.90}_{-1.55}$ | 8.037 |
| ID994 | $21.26^{+4.71}_{-3.85}$ | $56088.6^{+12418.2}_{-10167.1}$ | $16.01^{+3.54}_{-2.90}$ | 19.871 |
| ID995 | $14.35^{+3.18}_{-2.60}$ | $29022.0^{+6425.6}_{-5260.8}$ | $13.50^{+2.99}_{-2.45}$ | 14.230 |
| ID996 | $22.50^{+4.98}_{-4.08}$ | $49038.7^{+10857.3}_{-8889.2}$ | $18.48^{+4.09}_{-3.35}$ | 11.636 |
| ID997 | $5.42^{+1.20}_{-0.98}$ | $23537.5^{+5211.3}_{-4266.6}$ | $4.54^{+1.01}_{-0.82}$ | 12.562 |
| ID998 | $25.07^{+5.55}_{-4.55}$ | $19555.4^{+4329.6}_{-3544.8}$ | $18.81^{+4.16}_{-3.41}$ | 17.846 |
| ID999 | $5.70^{+1.26}_{-1.03}$ | $24024.9^{+5319.2}_{-4355.0}$ | $3.61^{+0.80}_{-0.65}$ | 23.020 |
| ID1000 | $39.23^{+8.69}_{-7.11}$ | $31835.1^{+7048.4}_{-5770.7}$ | $22.31^{+4.94}_{-4.04}$ | 15.884 |

**Note.** The catalog of 1000 simulated BBH inspiral events is used to test the inference of the BHMF from the data attainable with the ET. The reported values are the medians, with errors corresponding to the 16th and 84th percentiles, assuming $\alpha = 1.6$, $M_{\min} = 5M_\odot$, $M_{\max} = 50M_\odot$. Note that these mock data are resimulated with each realization.

### 3.1. Measurement Uncertainty

The intrinsic value of primary BH mass (i.e., $m_{1,\mathrm{fid}}$) follows a power-law distribution, however the measured $m_1$ is scattered by the log-normal distribution, which does not follow a power-law function anymore (Koen & Kondlo 2009). In theory, if the event $X$ follows a power-law distribution and its observed values are subject to log-normal uncertainty, then the observed event $X + e$, with $e$ denoting the error (uncertainty), is distributed according to the convolution of the power law and log-normal distribution. Assuming that the noised data follow the log-normal distribution, we convolved the intrinsic power law to describe likelihood as

$$P(\alpha, M_{\max}, M_{\min}|m_1) \propto \prod_{i=1}^{\mathrm{total}} \hat{P}(m_{1,i}|\alpha, M_{\max}, M_{\min}), \quad (8)$$

where $\hat{P}$ is the power-law function convolved with the log-normal distribution using a standard deviation of 0.2, as we assumed. We illustrate the effect of such a convolution in Figure 1.

### 3.2. Selection Effect

The GW observations have a tendency to discover more significant events, known as Malmquist bias. For example, the GW systems with higher values $m_1$ tend to produce stronger signals and thus have a higher probability of being detected. As a result, the final BHMFs are biased toward the high-mass end if this effect is not correctly taken into account.

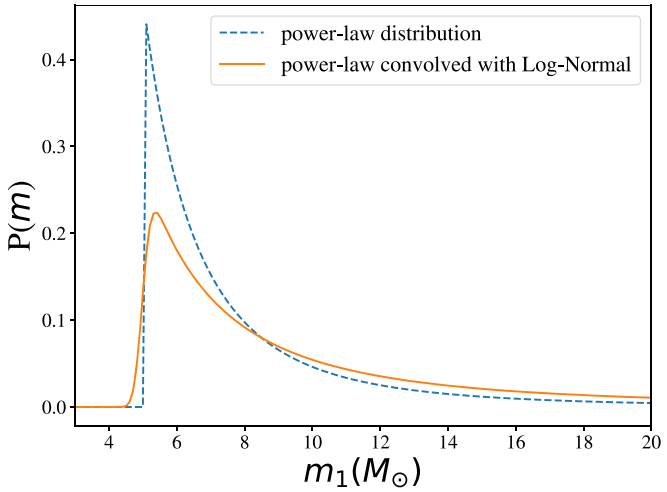


**Figure 1.** Convolution of a power-law distribution with a log-normal distribution with $\sigma = 0.2$. The convolution makes distribution shallower, smooths the breaking edge at $m_1 = 5M_\odot$, and makes the slope less steep.

To overcome this selection effect, we introduce the selection factor $\eta$ for the GW event, which is the detection probability of one event in a repeated simulation. The meaning of this factor $\eta$ is straightforward—if one GW event has $\eta = 0.2$, it means that this event has an 80% probability of being missed. In other words, four equivalent events would have been missed. Thus, for this event, one needs to recalibrate this influence by enhancing the likelihood by a power of 5 (i.e., $L^{1/0.2} = L^5$) to recover the intrinsic probability value. Hence, to account for the selection effect, we calculate the likelihood as

$$P(\alpha, M_{\max}, M_{\min}|m_1) \propto \prod_{i=1}^{\text{total}} \hat{P}(m_{1,i}|\alpha, M_{\max}, M_{\min})^{1/\eta}, \quad (9)$$

where $\eta$ is directly determined by the probability distribution of $\rho$, i.e., $\eta = P(\rho > 8)$. In order to use the Equation (1) to calculate $\rho$, the distribution function of $\Theta$ is taken from the MC simulations; the $\mathcal{M}_0$ and $d_L$ are adopted from the mock data set, as demonstrated in Table 1. Yet, the redshift $z_s$ is the unknown parameter since it is non-measurable in the GW detectors; one can only take the $d_L$ as a redshift estimator. Note that the observed $d_L$ and $\mathcal{M}_0$ are both considered to have random noise, which follows the asymmetric distribution (i.e., log-normal). Thus, the intrinsic probability distribution (not the errors to be convolved) of their product, and thus of $\eta$, is also asymmetric. Considering the random distributions of the $d_L$ and $\mathcal{M}_0$, we performed the numerical tests and found that the distribution of $1/\eta$ could be well described by the log-normal distribution with multiplicative standard deviation as $\sigma = -\log(\eta_{\text{median}})/3$; see Figure 2. Recall that in a log-normal distribution, the expected value is higher than the true value (i.e., median value) by a factor of $e^{\sigma^2/2}$. We consider this skewness and recalibrate the inferred expected value of $1/\eta$ to the median value, in order to assign a non-biased $1/\eta$ to the calculation.

### 3.3. Luminosity Distance as a Redshift Estimator

In the previous section, we took $d_L$ as the redshift estimator to derive the redshift and hence the selection factor $\eta$. Let us denote such an inferred redshift as $z_{\text{inf}}$. To derive $z_{\text{inf}}$, we take the observed luminosity distance, i.e., $d_L(z)$, and find the

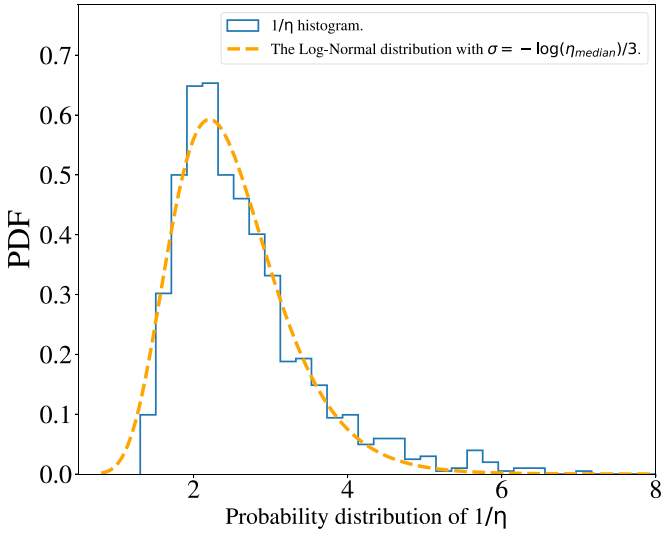


**Figure 2.** Assuming a set of $d_L$ and $\mathcal{M}_0$ following the log-normal distribution, we randomly produce a corresponding histogram of $1/\eta$ in order to assess its probability distribution. The result shows that the skewed distribution could be well described by a log-normal distribution with $\sigma = -\log(\eta_{\text{median}})/3$.

inverse solution of the integral function based on a fixed cosmological model.

Once the cosmological model is assumed, indirect inference of $z_s$ offers an opportunity to model the BHMF slope as a function of redshift. Therefore, we are able to investigate the second scenario described by Equation (5) as

$$P(\alpha_0, \alpha_1, M_{\max}, M_{\min}|m_1, d_L(z)) \propto \prod_{i=1}^{\text{total}} \hat{P}(m_{1i}, z_{\text{inf},i}|\alpha_0, \alpha_1, M_{\max}, M_{\min})^{1/\eta}. \quad (10)$$

We present our inference for the BHMF using the mock data in the next section.

## 4. Result

We fit the mock data to the BHMF model to infer the distribution of the best-fit parameters. To avoid the bias and estimate the scatter, we adopt the realization approach. In each realization, we simulate 1000 BBH inspiral GW events and infer the best-fit parameters using minimization of the chi-square objective function. We keep increasing the volume of realizations until the inferred best-fit parameters converge.

In the first scenario, we consider the slope $\alpha$ as a constant. We performed numerical tests assuming three different sets of parameters, taking $\alpha$ as 0.8, 1.6, and 2.4, with $M_{\min} = 5M_\odot$, $M_{\max} = 50M_\odot$. We calculate the likelihood with Equation (9) to infer the best-fit parameters in each realization. It has been discussed that no black holes with mass greater than $50M_\odot$ are expected from stellar evolution and through supernovae (Woosley 2017; Wiktorowicz et al. 2019). In Figure 3, we present the posterior distribution of the inferred parameters for the three parameter sets. We find that all the parameters are recovered accurately, which confirms the validity of our method. The uncertainties for the inferred parameters of the 68% confidence interval are $\Delta\alpha \sim 0.1$, $\Delta M_{\max} \sim 1$–$3M_\odot$ and $\Delta M_{\min} \sim 0.2$–$0.3M_\odot$. We also note that the uncertainty for $\Delta M_{\max}$ increases with increasing $\alpha$. This is reasonable given that for higher $\alpha$ values, the BH mass (i.e., $m_1$) tends to be distributed lower, resulting in a lower constraint power on the high-mass end. Clearly, the uncertainty levels cannot be treated as the universal range

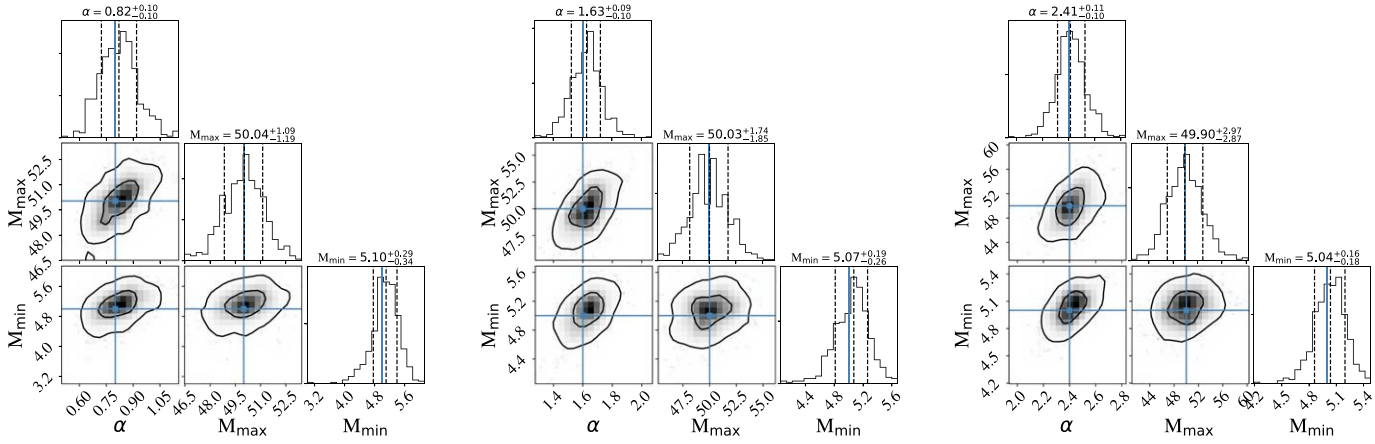


(a) assuming $\alpha = 0.8$, $M_{min} = 5M_{\odot}$ and $M_{max} = 50M_{\odot}$.

(b) assuming $\alpha = 1.6$, $M_{min} = 5M_{\odot}$ and $M_{max} = 50M_{\odot}$.

(c) assuming $\alpha = 2.4$, $M_{min} = 5M_{\odot}$ and $M_{max} = 50M_{\odot}$.

**Figure 3.** One- and two-dimensional distributions for the best-fitted parameters in the first scenario, based on three sets of parameters with 1000 BBH inspiral GW events. The BHMF is assumed as a power law with a hard cut at $M_{\rm min}$ and $M_{\rm max}$, and a constant slope ($\alpha$) across all the redshifts. The blue lines indicate the true value as assumed in the simulation.

for the general case, but only apply when the set of initial parameters is close to the tested ones. Moreover, these uncertainty levels are related to the assumed measurement uncertainties, including $\mathcal{M}_0$, $d_L$, and $m_1$, as discussed in Section 2.3.

In the second scenario, $\alpha$ evolves with redshift according to Equation (5). We consider four sets of parameters assuming $\alpha_0$ as 0.8, 1.6, 2.4, and $\alpha_1$, including 0.7 and 1.2. We present the results in Figure 4. The figure shows that all the assumed parameters can be recovered accurately. With one more parameter included in the second scenario, the uncertainty levels are as follows: $\Delta\alpha_0 \sim 0.4$, $\Delta\alpha_1 \sim 0.5$–$0.7$, $\Delta M_{\rm max} \sim 2$–$4M_{\odot}$, and $\Delta M_{\rm min} \sim 0.2$–$0.3M_{\odot}$. We note that there is a degeneracy between $\alpha_0$ and $\alpha_1$, which is understandable given that they are strongly related by Equation (5). However, for the four sets of parameters we tested, this degeneracy does not affect the inferred uncertainty level for $\alpha_0$ and $\alpha_1$.

We highlight that in this second scenario, it is the inferred uncertainty of $\alpha_1$ that matters the most. Our result shows that, with only 1000 GW measurements in the future, the inferred value of $\alpha_1$ would reach a precision of $\Delta\alpha_1 \sim 0.5$–$0.7$. Limited by the computing power, we could not use numerical tests to get a universal uncertainty level for the general case. However, given the four sets of tests as shown in Figure 4, it is likely that 1000 GW measurements could distinguish the evolution of the BHMF at the $1\sigma$ confidence level when $\alpha_1$ deviated from 0 by a value of 0.5. Moreover, we conjecture that the precision of an inference increases with the sample size as a function of $\sqrt{N}$. Thus, for the four sets of tests, the 1 year of ET measurements ($\sim 10^5$ in total) would decrease the uncertainty levels by a factor of 10. We also note that the distribution of the best-fitted parameters ($\alpha_0$, $\alpha_1$) does not follow the Gaussian distribution, but rather a large fraction of it is concentrated at the center.

## 5. Conclusion and Discussion

The third-generation gravitational-wave detector, the ET, is very powerful and capable of detecting $\sim 10^5$ GW events per year, at redshifts up to $z \sim 17$. In this study, we investigated how detections of the BBH mergers could improve our knowledge of the black hole mass function (BHMF).

We performed a MC simulation to estimate the uncertainty level of BHMF parameters inferred from GW signals by BBHs that would be detected by ET. As a starting point, we assumed that the BHMF for the primary BH mass followed a power-law distribution with hard cuts as described by Equation (4). Based on the BBH intrinsic merger rate predicted by `StarTrack`, we randomly simulated the key parameters of the BBH systems, including the chirp masses, redshifts, and orientation factor,s and calculated their corresponding signal-to-noise ratio $\rho$ for the ET. We collected the events whose $\rho$ exceeds the detecting threshold and injected log-normal noise into the detected parameter, including BH mass, chirp mass, and luminosity distance as mock data.

We built up a theoretical framework and explored using mock measurements to infer the BHMF. We took into account the measurement uncertainties and the selection effect, which could bias the inference. We performed the test using realizations, 1000 GW events adopted per realization, and estimated the distribution of the best-fitted parameters of the BHMF, including the power-law slope $\alpha$, the maximum BH mass $M_{\rm max}$ and the minimum BH mass $M_{\rm min}$ in the first scenario. Furthermore, in the second scenario, we considered $\alpha$ to evolve as a function of redshift as described by Equation (5), and used the luminosity distance as a redshift estimator to test this evolution. We summarize our main results as follows:

1. Using our method based on Equation (9), the tested parameters are all recovered accurately, as shown in Figure 3, which confirms the validity of our tests and highlights the importance of correctly considering the measurement uncertainty and selection effect.
2. We assumed $\alpha$ within a scenario in which it is evolving with redshift as $\alpha(z) = \alpha_0 + \alpha_1 \frac{z}{1+z}$. Taking the measured $d_L$ as a redshift estimator and testing with four parameter sets, we are able to recover the true value of $\alpha_1$ accurately, as shown in Figure 4.

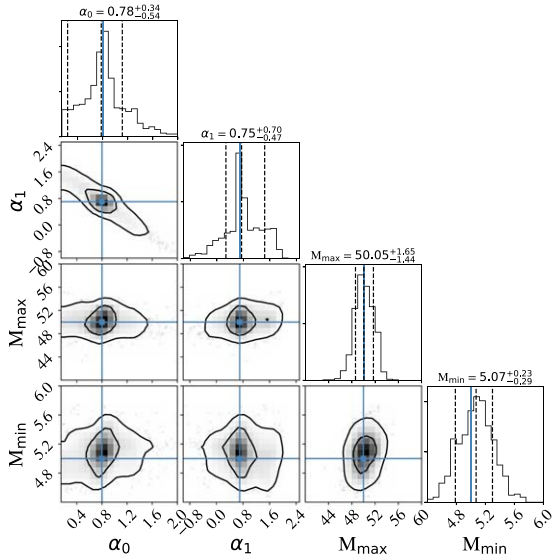


(a) assuming $\alpha_0 = 0.8$, $\alpha_1 = 0.7$, $M_{min} = 5M_\odot$ and $M_{max} = 50M_\odot$.

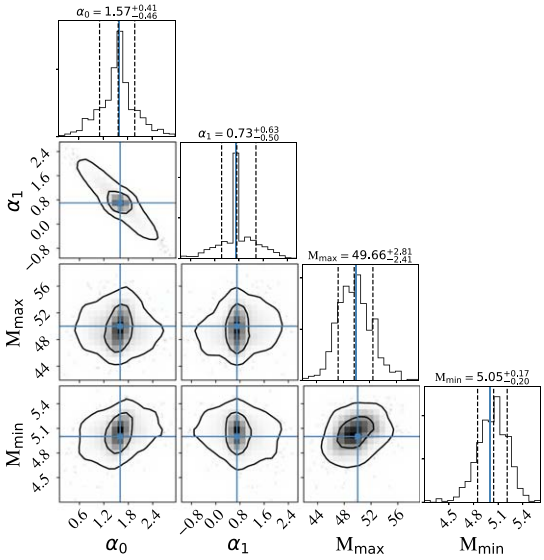


(b) assuming $\alpha_0 = 1.6$, $\alpha_1 = 0.7$, $M_{min} = 5M_\odot$ and $M_{max} = 50M_\odot$.

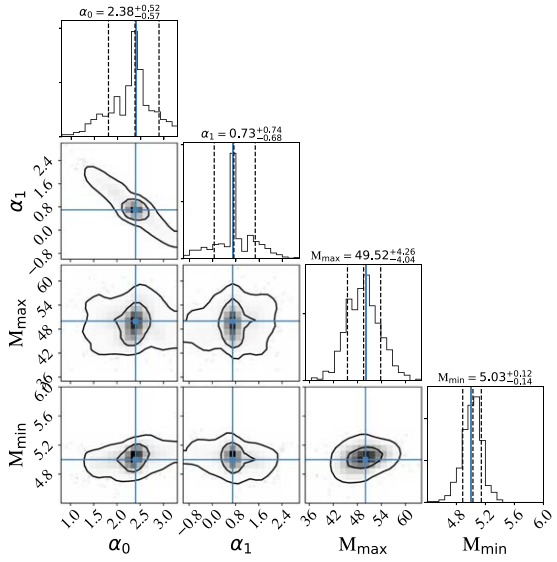


(c) assuming $\alpha_0 = 2.4$, $\alpha_1 = 0.7$, $M_{min} = 5M_\odot$ and $M_{max} = 50M_\odot$.

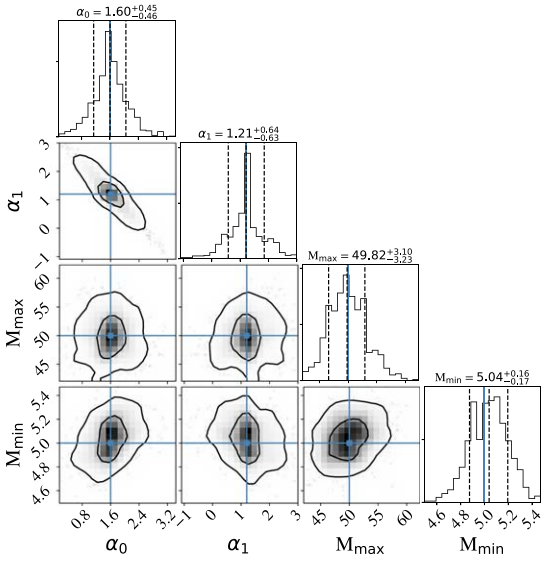


(d) assuming $\alpha_0 = 1.6$, $\alpha_1 = 1.2$, $M_{min} = 5M_\odot$ and $M_{max} = 50M_\odot$.

**Figure 4.** Same as Figure 3 but for the second scenario, where the $\alpha$ of the BHMF is evolving with redshift as $\alpha(z) = \alpha_0 + \alpha_1 \frac{z}{1+z}$; four sets of parameters are assumed.

3. Given the fixed sets of parameters, our results show that a volume of 1000 measurements of BBHs events could infer the parameters with uncertainties level at $\Delta\alpha \sim 0.1$, $\Delta M_{\rm max} \sim 1$–$2M_\odot$, and $\Delta M_{\rm min} \sim 0.2$–$0.3M_\odot$ for the first scenario. For the second scenario, the inferred uncertainties are $\Delta\alpha_0 \sim 0.4$, $\Delta\alpha_1 \sim 0.5$–$0.7$, $\Delta M_{\rm max} \sim 2$–$4M_\odot$, and $\Delta M_{\rm min} \sim 0.2 - 0.3M_\odot$. In the future, the 1 year detection rate of ET ($\sim 10^5$ in total) would increase the sample size by a factor of 100. If the precision of the inference increases with the sample size as a function of $\sqrt{N}$, we conclude that the one year BBH sample by ET would be able to deliver the parameters with uncertainties reduced by a factor of 10 with respect to those reported in this paper.

We point out a few circumstances that might weaken generality this work. First, we have adopted a template of intrinsic BBH merger rate based on the predictions by a standard model in `StarTrack`, which can be different from the realistic one. Of course, the intrinsic BBH merger rate is unknown, which is related to the lack of detailed knowledge of different variables such as BBH masses, explosion mechanism, metallicity history, and time delay distribution. With a different BBH merger rate template, the simulated mock events (i.e., the ones in the Table 1) would follow a different redshift distribution, which could slightly change the inference of the uncertainties of the inferred parameters. Second, for the sake of simplicity, we simulated the value of the secondary BH mass $m_2$ by assuming that two masses of BBHs have independent

distributions, which probably is not exactly true. One can expect that these two limitations would affect the prediction of the yearly detection rate of the GW events and their redshift distribution; however, their influence on our final inferred contours of the BHMF (i.e., Figures 3 and 4) is likely not very significant. The numerical tests done in this work confirmed the validity of our method. However, limited by the sets of tests, the uncertainty of the inferred parameters in both scenarios applies directly to the fixed sets of parameters and should not be applied to the general case.

In this work, we focused on the inference of the BHMF using the mass properties of the BBH. However, it is worth noting that our approach could be extended to address other problems. For example, one could infer the spin of the BH (The LIGO Scientific Collaboration & The Virgo Collaboration 2019b), and the mass function for the binary of the NS–NS, NS-BH system, though these events are detectable at lower redshift ($z < 4$). In addition, using the luminosity as a redshift estimator, one should also be able to reconstruct the BBH intrinsic merger rate (Fishbach et al. 2018) and the cosmological parameters.

We thank Hosek Jr., M.W. for a useful discussion.

This work was supported by the National Natural Science Foundation of China under grants No. 11633001 and 11920101003, the Strategic Priority Research Program of the Chinese Academy of Sciences, grant No. XDB23000000, and the Interdiscipline Research Funds of Beijing Normal University.

X. Ding acknowledges support by the China Postdoctoral Science Foundation (No. 2017M622501). M.B. was supported by the Key Foreign Expert Program for the Central Universities No. X2018002. K. Liao was supported by the National Natural Science Foundation of China (NSFC; No. 11973034).

*Software:* CORNER, (Foreman-Mackey 2016), Matplotlib (Hunter 2007), and standard Python libraries.

## ORCID iDs

Xuheng Ding https://orcid.org/0000-0001-8917-2148
Kai Liao https://orcid.org/0000-0002-4359-5994
Marek Biesiada https://orcid.org/0000-0003-1308-7304
Zong-Hong Zhu https://orcid.org/0000-0002-3567-6743

## References

Abernathy, M., Acernese, F., Ajith, P., et al. 2011, Document Number ET-0106A-10, http://www.et-gw.eu/index.php/etdsdocument
Bethe, H. A., & Brown, G. E. 1998, ApJ, 506, 780
Biesiada, M., Ding, X., Piórkowska, A., & Zhu, Z.-H. 2014, JCAP, 2014, 080
Cai, R.-G., & Yang, T. 2017, PhRvD, 95, 044024
Collett, T. E., & Bacon, D. 2017, PhRvL, 118, 091101
de Mink, S. E., & Mandel, I. 2016, MNRAS, 460, 3545
Ding, X., Biesiada, M., Zheng, X., et al. 2019, JCAP, 2019, 033
Ding, X., Biesiada, M., & Zhu, Z.-H. 2015, JCAP, 2015, 006
Dominik, M., Belczynski, K., Fryer, C., et al. 2013, ApJ, 779, 72
Fan, X.-L., Liao, K., Biesiada, M., Piórkowska-Kurpas, A., & Zhu, Z.-H. 2017, PhRvL, 118, 091102
Finn, L. S., & Chernoff, D. F. 1993, PhRvD, 47, 2198
Fishbach, M., Holz, D. E., & Farr, W. M. 2018, ApJL, 863, L41
Foreman-Mackey, D. 2016, corner.py: corner.py v1.0.2, Zenodo, doi:10.5281/zenodo.45906
Fryer, C. L. 1999, ApJ, 522, 413
Fryer, C. L., & Kalogera, V. 2001, ApJ, 554, 548
Ghosh, A., Del Pozzo, W., & Ajith, P. 2016, PhRvD, 94, 104070
Hunter, J. D. 2007, CSE, 9, 90
Koen, C., & Kondlo, L. 2009, MNRAS, 397, 495
Kormendy, J., & Richstone, D. 1995, ARA&A, 33, 581
Kovetz, E. D., Cholis, I., Breysse, P. C., & Kamionkowski, M. 2017, PhRvD, 95, 103010
Kulkarni, S. R., Hut, P., & McMillan, S. 1993, Natur, 364, 421
Liao, K., Fan, X.-L., Ding, X., Biesiada, M., & Zhu, Z.-H. 2017, NatCo, 8, 2136
Lynden-Bell, D. 1969, Natur, 223, 690
Marchant, P., Langer, N., Podsiadlowski, P., Tauris, T. M., & Moriya, T. J. 2016, A&A, 588, A50
Mirabel, F. 2017, NewAR, 78, 1
Piórkowska, A., Biesiada, M., & Zhu, Z.-H. 2013, JCAP, 2013, 022
Portegies Zwart, S. F., & McMillan, S. L. W. 2000, ApJL, 528, L17
Portegies Zwart, S. F., & Yungelson, L. R. 1998, A&A, 332, 173
Taylor, S. R., & Gair, J. R. 2012, PhRvD, 86, 023502
The LIGO Scientific Collaboration, & The Virgo Collaboration, 2016a, PhRvL, 116, 061102
The LIGO Scientific Collaboration, & The Virgo Collaboration, 2016b, PhRvX, 6, 041015
The LIGO Scientific Collaboration, & The Virgo Collaboration, 2017, AnP, 529, 1600209
The LIGO Scientific Collaboration, & The Virgo Collaboration, 2019a, PhRvX, 9, 031040
The LIGO Scientific Collaboration, & The Virgo Collaboration, 2019b, ApJL, 882, L24
Wiktorowicz, G., Wyrzykowski, Ł., Chruslinska, M., et al. 2019, ApJ, 885, 1
Woosley, S. E. 2017, ApJ, 836, 244
Yang, L., Ding, X., Biesiada, M., Liao, K., & Zhu, Z.-H. 2019, ApJ, 874, 139